DOI: 10.21122/2220-9506-2025-16-2-87-97

Disordered Tin Oxide Films for Thermoelectric Applications: Correlation between Microstructure, Electrical Conductivity and Seebeck Coefficient

V.K. Ksenevich[1], V.A. Dorosinets[1], M.A. Samarina[1], N.A. Poklonski[1], I.A. Svito[1], D.V. Adamchuk[2], G. Abdurakhmanov[3]

[1]*Belarusian State University,*
Nezavisimosti Ave., 4, Minsk 220030, Belarus

[2]*Institute for Nuclear Problems of Belarusian State University,*
Bobruiskaya str., 11, Minsk 220030, Belarus

[3]*National University of Uzbekistan named after Mirzo Ulugbek,*
Universitetskaya str., 4, Tashkent 100174, Uzbekistan

Received 24.04.2025
Accepted for publication 05.06.2025

Abstract

The aim of the work was to establish a correlation between structural, electrical and thermoelectric properties of the disordered tin oxide films to study the possibility of their further applications as materials for thermoelectric converters. Disordered multiphase tin oxide films were synthesized by magnetron sputtering of tin onto glass substrates in argon plasma and subsequent two-stage annealing in air. The structural, electrical and thermoelectric properties of the films were varied by changing the temperature at the 2nd stage of annealing in the range of 350–450 °C. It was found that the films synthesized at a temperature of 350 °C during the 2nd stage of annealing procedure have an amorphous structure and are characterized by the highest value of specific electrical conductivity $\sigma \approx 28.5$ S/m. Samples fabricated at temperatures 400 and 450 °C during the 2nd stage of annealing are characterized by polycrystalline multiphase structure with both stoichiometric (SnO, SnO_2) and non-stoichiometric (Sn_2O_3 and Sn_3O_4) phases of tin oxides in their composition (with prevailing of SnO_2 phase for the samples annealed at 450 °C). It was found that these samples are characterized by a higher value of the Seebeck coefficient S (–156 μV/K and –163 μV/K, respectively) compared to the amorphous films, for which the value $S = –90$ μV/K. It was found that the electrical conductivity of both amorphous and polycrystalline tin oxide films in the temperature range of ≈ 80–300 K can be described within the frame of a model that assumes the activation of electrons from impurity levels in the band gap associated with oxygen vacancies in different charge states. It was demonstrated that for all types of the samples, the Pisarenko's formula can be applied to evaluate the relationship between the Seebeck coefficient S and the position of the Fermi level E_F if the parameter $r < –2$.

Keywords: magnetron sputtering, tin oxide films, electrical conductivity, thermal activation, thermoEMF coefficient

Адрес для переписки:
Ксеневич В.К.
Белорусский государственный университет,
пр. Независимости, 4, г. Минск 220030, Беларусь
e-mail: ksenevich@bsu.by

Address for correspondence:
Ksenevich V.K.
Belarusian State University,
Nezavisimosti Ave., 4, Minsk 220030, Belarus
e-mail: ksenevich@bsu.by

Для цитирования:
V.K. Ksenevich, V.A. Dorosinets, M.A. Samarina, N.A. Poklonski, I.A. Svito, D.V. Adamchuk, G. Abdurakhmanov.
Disordered Tin Oxide Films for Thermoelectric Applications: Correlation between Microstructure, Electrical Conductivity and Seebeck Coefficient.
Приборы и методы измерений.
2025. Т. 16. № 2. С. 87–97.
DOI: 10.21122/2220-9506-2025-16-2-87-97

For citation:
Ksenevich VK, Dorosinets VA, Samarina MA, Poklonski NA, Svito IA, Adamchuk DV, Abdurakhmanov G.
Disordered Tin Oxide Films for Thermoelectric Applications: Correlation between Microstructure, Electrical Conductivity and Seebeck Coefficient.
Devices and Methods of Measurements.
2025;16(2):87–97.
DOI: 10.21122/2220-9506-2025-16-2-87-97

DOI: 10.21122/2220-9506-2025-16-2-87-97

Неупорядоченные плёнки оксидов олова для термоэлектрических применений: корреляция между микроструктурой, электропроводностью и коэффициентом Зеебека

В.К. Ксеневич[1], В.А. Доросинец[1], М.А. Самарина[1], Н.А. Поклонский[1], И.А. Свито[1], Д.В. Адамчук[2], Г. Абдурахманов[3]

[1]*Белорусский государственный университет,*
пр-т Независимости, 4, г. Минск 220030, Беларусь

[2]*Институт ядерных проблем Белорусского государственного университета,*
ул. Бобруйская, 11, г. Минск 220030, Беларусь

[3]*Национальный университет Узбекистана имени Мирзо Улугбека,*
ул. Университетская, 4, г. Ташкент 100174, Узбекистан

Поступила 24.04.2025
Принята к печати 05.06.2025

Цель работы – установление взаимосвязи между структурными, электрическими и термоэлектрическими свойствами неупорядоченных плёнок оксидов олова для определения возможности дальнейшего их применения в качестве материалов для термоэлектрических преобразователей. Неупорядоченные многофазные плёнки оксидов олова синтезированы методом магнетронного распыления олова на стеклянные подложки в плазме аргона с последующим двухстадийным отжигом на воздухе. Структурные, электрические и термоэлектрические свойства плёнок варьировались посредством изменения температуры на 2-й стадии отжига в диапазоне 350–450 °С. Установлено, что плёнки, синтезированные при температуре 350 °С на 2-й стадии отжига, имеют рентгеноаморфную структуру и характеризуются наибольшей величиной удельной электропроводности σ ≈ 28,5 См/м. Структура образцов, полученных при температурах 400 и 450 °С на 2-й стадии отжига, является поликристаллической многофазной, с наличием в их составе как стехиометрических (SnO, SnO_2), так и нестехиометрических (Sn_2O_3 и Sn_3O_4) фаз оксидов олова (с преобладанием фазы SnO_2 при отжиге при 450 °С). При этом эти образцы характеризуются большей величиной коэффициента Зеебека S (–156 мкВ/К и –163 мкВ/К соответственно) по сравнению с рентгеноаморфными плёнками, для которых величина $S = –90$ мкВ/К. Установлено, что электропроводность как аморфных, так и поликристаллических плёнок оксидов олова в диапазоне температур ≈ 80–300 К может быть описана в рамках модели, предполагающей активацию электронов с примесных уровней в запрещённой зоне, связанных с кислородными вакансиями в различных зарядовых состояниях. Показано, что для всех исследованных образцов для оценки взаимосвязи между коэффициентом Зеебека S и положением уровня Ферми E_F может быть применена формула Писаренко при условии, что параметр $r < –2$.

Ключевые слова: магнетронное распыление, плёнки оксидов олова, электропроводность, термическая активация, коэффициент термоЭДС

Адрес для переписки:
Ксеневич В.К.
Белорусский государственный университет,
пр. Независимости, 4, г. Минск 220030, Беларусь
e-mail: ksenevich@bsu.by

Address for correspondence:
Ksenevich V.K.
Belarusian State University,
Nezavisimosti Ave., 4, Minsk 220030, Belarus
e-mail: ksenevich@bsu.by

Для цитирования:
V.K. Ksenevich, V.A. Dorosinets, M.A. Samarina, N.A. Poklonski, I.A. Svito, D.V. Adamchuk, G. Abdurakhmanov.
Disordered Tin Oxide Films for Thermoelectric Applications: Correlation between Microstructure, Electrical Conductivity and Seebeck Coefficient.
Приборы и методы измерений.
2025. Т. 16. № 2. С. 87–97.
DOI: 10.21122/2220-9506-2025-16-2-87-97

For citation:
Ksenevich VK, Dorosinets VA, Samarina MA, Poklonski NA, Svito IA, Adamchuk DV, Abdurakhmanov G.
Disordered Tin Oxide Films for Thermoelectric Applications: Correlation between Microstructure, Electrical Conductivity and Seebeck Coefficient.
Devices and Methods of Measurements.
2025;16(2):87–97.
DOI: 10.21122/2220-9506-2025-16-2-87-97

Introduction

Thermoelectric (TE) generators are used for recovery of electrical energy from waste heat. Research in this field has grown significantly over the past decades due to fossil energy resource depletion. Solid-state thermoelectric energy converters are used as sources of electricity in portable devices, as well as in electronic, medical, scientific equipment, on spacecraft, etc. [1, 2].

The efficiency of TE devices is estimated by the dimensionless parameter of thermoelectric figure of merit:

$$ZT = S^2\sigma T/\kappa, \quad (1)$$

where S, σ and κ are the Seebeck coefficient, electrical and thermal conductivity of the TE material, respectively; T is the operating temperature or average temperature $(T_1 + T_2)/2$ of the TE converter; T_1 and T_2 are the temperatures of its hot and cold contacts, respectively [3].

Parameters of Seebeck coefficient S and electrical conductivity σ in the numerator of Eq. (1) are determined only by the electronic properties of materials, therefore they are often combined into the quantity $PF = S^2\sigma$, called "Power factor". The value of thermal conductivity κ in the denominator of Eq. (1) can be considered as a sum of 2 terms [3]:

$$\kappa = \kappa_L + \kappa_e, \quad (2)$$

where κ_L and κ_e are the contributions from the lattice and electronic component of heat conductivity.

According to (1), it is obvious, that for high efficiency of heat to electricity conversion TE materials should have a high electrical conductivity σ, a high Seebeck coefficient S, and a low thermal conductivity κ.

Increasing the value of thermoelectric figure of merit of thermoelectric materials is a rather complicated task, requiring the fulfillment of contradictory conditions (increasing electrical conductivity while simultaneously reducing thermal conductivity).

In order to achieve maximum figure of merit value highly doped semiconductors and semimetals are usually used as a thermoelectric materials due to optimal relations between values of electrical conductivity σ, thermal conductivity κ and Seebeck coefficient S in them [4]. However, non-degenerate electronic materials can be characterized by high figure of merit value as well [4].

Possibility of high values of Seebeck coefficient and figure of merit in disordered materials near metal–insulator transition is demonstrated in [5]. In such materials electrical conductivity is explained by transfer of localized electrons in the vicinity of the Fermi level.

The disadvantage of using non-degenerate semiconductors as TE materials is related to their low electrical conductivity. From the other side these materials are characterized by higher value of Seebeck coefficient S and low value of electronic term of the thermal conductivity κ_e. For these materials value of lattice term of heat conductivity κ_L can be comparable or even higher than the parameter κ_e. That is why one of the efficient methods to increase the figure of merit of TE materials is to reduce their lattice term of the thermal conductivity κ_L, characterizing the transfer of heat energy by phonons.

One of the most successful strategies for fabrication of TE materials with low value of the lattice thermal conductivity is the synthesis of structurally inhomogeneous samples [3, 6, 7]. Nanostructured materials (quantum wires, quantum dots, quantum wells) as well as materials with different types of nanoscale inclusions can be used as a materials with low κ_L value. For example, it was found that κ_L value of Si nanowire is much times less than lattice thermal conductivity of bulk Si (2 W/m·K vs 87.3 W/m·K respectively) [8]. However, for the fabrication of ordered low-dimensional structures a complicated and expensive technological equipment is required. Therefore, technologies based on the synthesis of non-homogeneous semiconductors as well as on the introducing of different types of point, linear and planar defects into the film and bulk semiconductors are considered as effective methods for the fabrication of TE materials with low lattice thermal conductivity value [9]. Mean free path of phonons can be reduced due to the scattering by point defects, dislocations, crystallite boundaries and nanoparticles of various phases [9]. It was found, for example, that nanocrystalline Si have much lower value of κ_L = 6.3 W/m·K in comparison with the bulk Si [10].

Widely used at present time commercial TE generators contain either expensive (Bi, Te, Ag and Se) or toxic (Pb, Hg) elements [11–13]. Besides that, chalcogenides are unstable in air and can be decomposed at relatively low temperatures. Therefore, protection from the influence of atmosphere for TE generators based on chalcogenides is required. As a result, manufacturing technology of such devices becomes more complicated and their price is increased.

As one of possible alternative to chalcogenides the metal oxides are considered [14, 15]. These materials are characterized by low cost, wide availability, environmental friendliness and stability at high temperatures. This explains their wide application in optoelectronics, photovoltaics, sensorics etc. One of the most widely used metal oxide is tin dioxide SnO_2. In the stoichiometric composition SnO_2 is a wide band gap (E_g = 3.6 eV) semiconductor characterized by very low electrical conductivity σ [16]. Increasing of parameter σ can be achieved not only by doping, but by means of introducing of oxygen vacancies as a source of electrons during synthesis process. It is known that oxygen vacancies introduce shallow donor levels in the band gap of SnO_2 [17]. It is possible to synthesize tin dioxide samples with high concentration of electrons only by means of variation of technological procedure parameters resulting in fabrication of electrically degenerate semiconductors without need for additional atomic doping [18]. Tin oxide thin films have advantages in comparison with bulk oxide materials due to possibility to tune concentration of necessary defects by more controllable way.

Previous studies of thermoelectric properties of tin monooxide SnO [19–21] and tin dioxide SnO_2 [20–26] films have shown that these materials can be considered as perspective candidates for development of thermoelectric converters on their basis. A major challenge in producing efficient thermoelectric generators using these materials is their high lattice thermal conductivity (κ_L), arising from the strong ionic bonds in oxides and the low atomic mass of oxygen atoms.

Analysis of thermoelectric properties of tin monoxide and tin dioxide was carried out in [21]. In particular, the similarity of the electronic vibrational states of SnO and SnSe (characterized by high value of ZT = 2.6 at 923 K) was noted. Such high value of ZT in SnSe can be explained by extremely low value of the electron component of thermal conductivity κ_e = 0.23 W/m·K due to strong lattice anharmonicity caused by the bound chemically active electron pairs arising as a result of the interaction of the Sn(5*p*) state and the antibonding state Sn(5*s*)-Se(*p*) [27]. Similar to selenium, oxygen is also in group 6 of the periodic table, which suggests that SnO contains a similar bound electron pair as found in SnSe. As a thermoelectric material, SnO presents several advantages compared to SnSe, particularly considering selenium's high toxicity and limited production volumes. Research [20] shows the feasibility of developing thermoelectric touch sensors using *p*-type SnO_x films.

It should be noted that amorphous tin oxides show promise as potential thermoelectric materials [15]. These materials exhibit high electron mobility due to the overlapping of spherically symmetric Sn 5*s* orbitals. Consequently, amorphous SnO_x samples can achieve higher electrical conductivity σ compared to their crystalline counterparts. Moreover, the disordered structure of amorphous samples results in lower thermal conductivity κ than that observed in crystalline materials of identical chemical composition.

While the thermoelectric parameters and their relationship with electrical conductivity in crystalline materials are described by well-known formulas [28], structural disorder significantly affects both the electrical conductivity and the Seebeck coefficient S of thermoelectrical materials. Our efforts in this work were focused on the investigation of the electrical conductivity and Seebeck coefficient S of undoped tin oxides films with different disorder degree and various phase composition. Previously, we developed a method of fabrication of tin oxide films [29–33] that allows control over their crystalline structure (ranging from amorphous to polycrystalline, including various stoichiometric and non-stoichiometric phases) and electrical conductivity σ spanning from near-insulating values to those characteristic of degenerate disordered semiconductors and disordered metals.

The aim of this work was to establish the correlation between the structural properties, electrical conductivity σ and Seebeck coefficient S in disordered tin oxides films and to test the feasibility of the relationship between thermoelectric and electrical parameters inherent for crystalline materials for the case of tin oxide based semiconductors with a disordered crystalline lattice.

Experimental details

AC magnetron sputtering of tin target (with purity 99.99 %) in argon plasma followed by two-stage oxidative annealing in air of deposited onto the glass substrate tin films was used for synthesis of disordered tin oxide films [34]. The following parameters were used during magnetron deposition process: the tin target diameter was 10 cm, the target-substrate distance was 4 cm, the voltage applied to the target

was 380 V, the pulse repetition rate of AC power supply was 70 kHz. Two-stage oxidative annealing of the deposited tin films was carried out at 200 °C for 2 hours at the 1st stage, followed by an increase in temperature to 350, 400 or 450 °C and isothermal annealing for 1 hour at the 2nd stage. The temperature of the 2nd stage of annealing was varied in order to change the structure, electrical conductivity σ and thermoelectric coefficient *S* of the films.

The structural properties of disordered tin oxide films were characterized by X-ray diffraction analysis using an Ultima IV RIGAKU X-ray diffractometer in a sliding beam geometry (α = 3°) using monochromatic CuKα copper radiation (λ = 0.154178 nm) and a high-speed D/teX X-ray detector.

The Raman spectra of tin oxide films were measured using a spectral-analytical system Nanofinder HE with excitation by a laser with a wavelength λ = 532 nm. Measurements were carried out at room temperature in the backscattering configuration. The resolution of spectrometer was 3 cm^{-1}, the diameter of the beam spot was about 1 μm, and the input power was about 0.6 mW.

Indium contacts were soldered to the samples using an ultrasonic soldering for possibility to study the electrical and thermoelectric properties of the films. The temperature dependences of the electrical conductivity σ(*T*) were measured in the nitrogen vessel in the temperature range of ≈ 80–300 K using the four-probe measurements technique. The Seebeck coefficient *S* measurements were carried out at temperatures in the range 298–300 K in a thermoelectric power cell with a temperature gradient varied from 0.2 to 7 K between the cold and hot ends of the film.

Experimental results and discussion

The influence of the 2nd stage annealing temperature on the crystalline structure and phase composition of synthesized tin oxide films was studied using X-ray diffraction analysis and Raman spectroscopy [34]. The XRD patterns of the tin oxide films samples fabricated at various 2nd stage annealing temperatures (350, 400 and 450 °C) are shown in Figure 1.

The diffraction patterns of the studied samples demonstrate that the applied synthesis method allows the formation of amorphous or polycrystalline multiphase films of tin oxides (including tin monoxide SnO of tetragonal structure, tin dioxide SnO_2 of tetragonal structure of the rutile type, as well as non-stoichiometric phases Sn_2O_3 and Sn_3O_4) [30, 33–36].

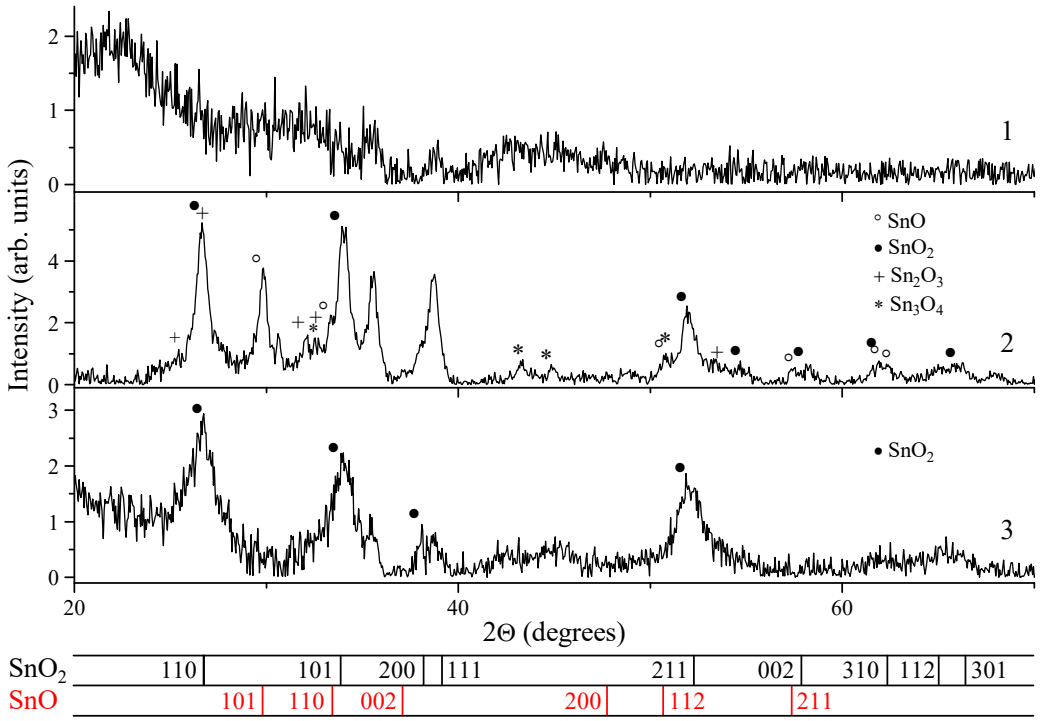

Figure 1 – XRD patterns of the tin oxide films deposited by magnetron sputtering of tin onto glass substrates in an argon atmosphere, followed by two-stage annealing in air: at 200 °C for 2 hours (1st stage) and at 350 °C (1), 400 °C (2) or 450 °C (3) for 1 hour (2nd stage)

In particular, as one can see from Figure 1, films fabricated at 350 °C are characterized by amorphous structure. Tin oxide films synthesized at the temperature 400 °C on the 2nd stage of the annealing procedure exhibited a polycrystalline structure containing both stoichiometric (SnO, SnO_2) and nonstoichiometric (Sn_2O_3, Sn_3O_4) phases. X-ray diffraction patterns of these films showed predominant reflections corresponding to the SnO_2 phase. The most intense peaks near 26.6°, 33.9° and 51.8° can be assigned to the X-ray reflections from the (110), (101) and (211) planes of the SnO_2 tetragonal rutile structure, respectively. The peaks observed around 29.9°, 33.3°, 50.7° and 57.4° correspond to the reflections from the (101), (110), (112) and (211) planes of the tetragonal structure of tin monoxide SnO, suggesting incomplete oxidation of tin films annealed at 400 °C. Increasing of the annealing temperature to 450 °C leads to the formation of tin oxide films with prevailing of SnO_2 tetragonal rutile structure. However, broadening of the peaks near 26.6°, 33.9° and 51.8° related to the X-ray reflections from (110), (101) and (211) planes of this structure indicates the formation of more disordered crystalline structure.

The sizes of SnO_2 crystallites for films annealed at 400 and 450 °C were estimated from the full-width at half-maximum (FWHM) intensity of the observed peaks using the Debye–Scherrer equation in the form [35]:

$$D = K\lambda/\beta\cos\theta, \quad (3)$$

where K is the shape factor which is usually equal to 0.89; λ is the radiation wavelength of CuKα equal to 0.154178 nm; θ is the Bragg diffraction angle; β is the full-width at half maximum (FWHM) of diffraction peak. It was found that crystallites sizes for films annealed at 400 °C are ranging from 10.4 to 13.6 nm, approximately twice the size of crystallites in films annealed at 450 °C (5.6–6.9 nm).

Thus, XRD analysis demonstrated that increasing of the temperature on the 2nd stage of the annealing procedure leads to the essential change of the crystalline structure of the synthesized samples. By means of variation of this technological parameter we can fabricate both amorphous and polycrystalline tin oxide films. Moreover, content of SnO, SnO_2, Sn_2O_3 and Sn_3O_4 phase and crystallites size can be tuned as well by adjusting the 2nd stage annealing temperature.

Strong influence of the annealing temperature on the structural properties of the synthesized tin oxide films is confirmed by the Raman spectra of the samples shown in Figure 2. Raman spectra of films prepared during the 2nd annealing stage at 350 °C showed no characteristic peaks associated with the vibrational modes of either stoichiometric (SnO, SnO_2) or non-stoichiometric (Sn_2O_3, Sn_3O_4) crystalline tin oxide phases. Only two broad bands are observed in the Raman spectra of these samples. It is possible to distinguish only some low-intensive lines, for example, near 76, 172 and 470 cm^{-1} (related to the pairs of A_g and B_g vibrational modes of Sn_3O_4), near 204 cm^{-1} (related to the A_{1g} vibrational mode of SnO), near 299 cm^{-1} (related to the vibrational modes of Sn_2O_3) [16, 34, 36, 37]. For films obtained at temperatures of 400 and 450 °C at the 2nd stage of annealing, the Raman spectra exhibit characteristic lines of stoichiometric phases SnO (near 204 and 350 cm^{-1}) and SnO_2 (near 630 cm^{-1}), as well as the non-stoichiometric phases Sn_2O_3 (near 76, 299 and 470 cm^{-1}) and Sn_3O_4 (near 172 and 700 cm^{-1}) [37]. These features of Raman spectra correlate with the XRD patterns typical for amorphous and polycrystalline structures, confirming significant structural disorder of these samples.

It was found that the temperature of the 2nd stage annealing procedure of the samples affected not only their structural but also the electrical properties. The measurements of electrical conductivity σ demonstrated that the highest value σ ≈ 28.5 S/m is inherent to the amorphous tin oxide films. This fact can be explained by high mobility of charge carriers μ due to the overlap of spherically symmetric 5*s* orbitals of Sn atoms [15] and by high concentration of oxygen vacancies [18], which form donor energy levels in the forbidden band of SnO_2 phase, the most electrically conductive phase of the samples. The lowest value of σ, equal to 2.1 S/m, observed for films synthesized at 450 °C is associated with the low concentration of oxygen vacancies due to more effective oxidation processes at high temperatures. Structural analysis further confirms that these polycrystalline films are characterized by small crystallite sizes, which enhances electron scattering at grain boundaries.

It should be noted that all types of the samples are characterized by *n*-type of electrical conductivity as indicated by the negative sign of the Seebeck coefficient measurements. Polycrystalline films annealed at 400 and 450 °C during the 2nd annealing stage exhibit higher Seebeck coefficients (S = –156 μV/K and –160 μV/K, respectively) compared to the most conductive sample annealed at 350 °C (S = –90 μV/K).

Temperature dependences of the electrical conductivity of all 3 types of the films are shown in Figure 3 in the scale σ(1/T). As one can see in Figure 3,

in spite of the differences in the values of specific electrical conductivity σ of the samples synthesized at different temperatures at the 2nd stage of the annealing procedure, the temperature dependences of the electrical conductivity of all films can be approximated using the same standard equation that takes into account the presence of two donor levels in the band gap of films [38, 39]:

$$\sigma(T) = A \cdot \exp\left(-\frac{\varepsilon_1}{k_B T}\right) + B \cdot \exp\left(-\frac{\varepsilon_2}{k_B T}\right), \quad (4)$$

where A and B are temperature independent parameters; k_B is Boltzmann constant, ε_1 and ε_2 are the energy of activation of electrons from the donor levels.

Table below lists the key electrical and thermoelectrical parameters of the tin oxide films: specific electrical conductivity (σ), Seebeck coefficient (S), activation energies (ε_1 and ε_2), and power factor (PF). Activation energies ε_1 and ε_2 in our samples can be related to the donor impurity levels formed by oxygen vacancies in two different charge states in SnO_2 [40]. Based on the analysis of the $\sigma(T)$ dependences of tin oxide films, we can conclude that the primary mechanism of electrical conductivity in both amorphous and polycrystalline samples within the temperature range of approximately 80–300 K is the thermal activation of electrons from impurity levels. These levels can be associated with oxygen vacancies in two different charge states within the SnO_2 structure.

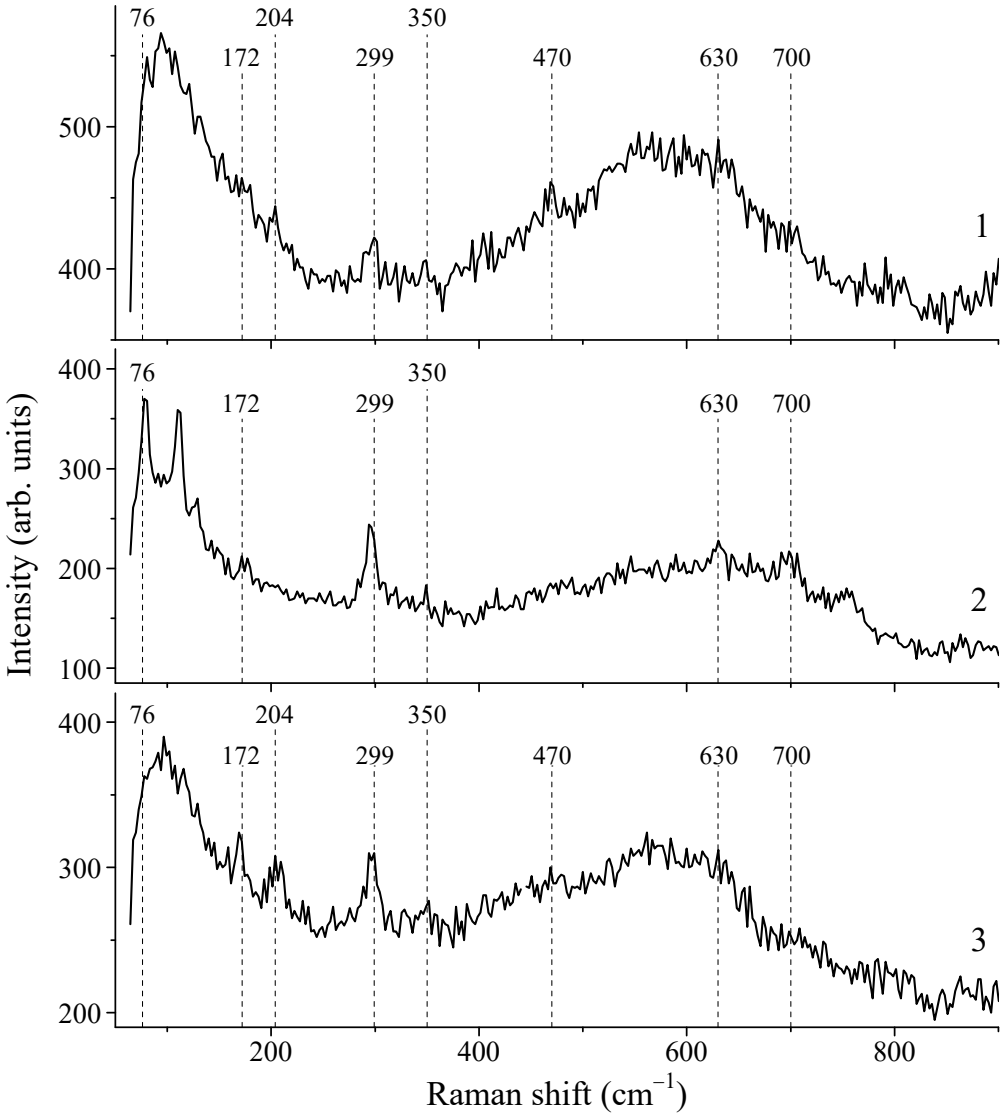

Figure 2 – Raman spectra of the tin oxide films deposited by magnetron sputtering of tin onto glass substrates in an argon atmosphere, followed by two-stage annealing in air: at 200 °C for 2 hours (1st stage) and at 350 °C (1), 400 °C (2) or 450 °C (3) for 1 hour (2nd stage)

Table

Values of specific electrical conductivity σ, Seebeck coefficient *S*, activation energies ε_1 and ε_2 and power factor PF of the tin oxide films deposited on glass substrates by magnetron sputtering of tin in argon atmosphere with the following annealing in air at 200 °C for 2 hours at the 1st stage and at T_{a2} = 350, 400 and 450 °C for 1 hour at the 2nd stage

T_{a2}, °C	Crystalline structure	σ, S/m	*S*, μV/K	ε_1, meV	ε_2, meV	PF, mW/m·K^2
350	Amorphous	28.5	–90	4.7	34.6	$2.31\cdot10^{-4}$
400	Polycrystalline	11.5	–156	30.3	84.6	$2.80\cdot10^{-4}$
450	Polycrystalline	2.1	–163	39.9	97.2	$5.6\cdot10^{-5}$

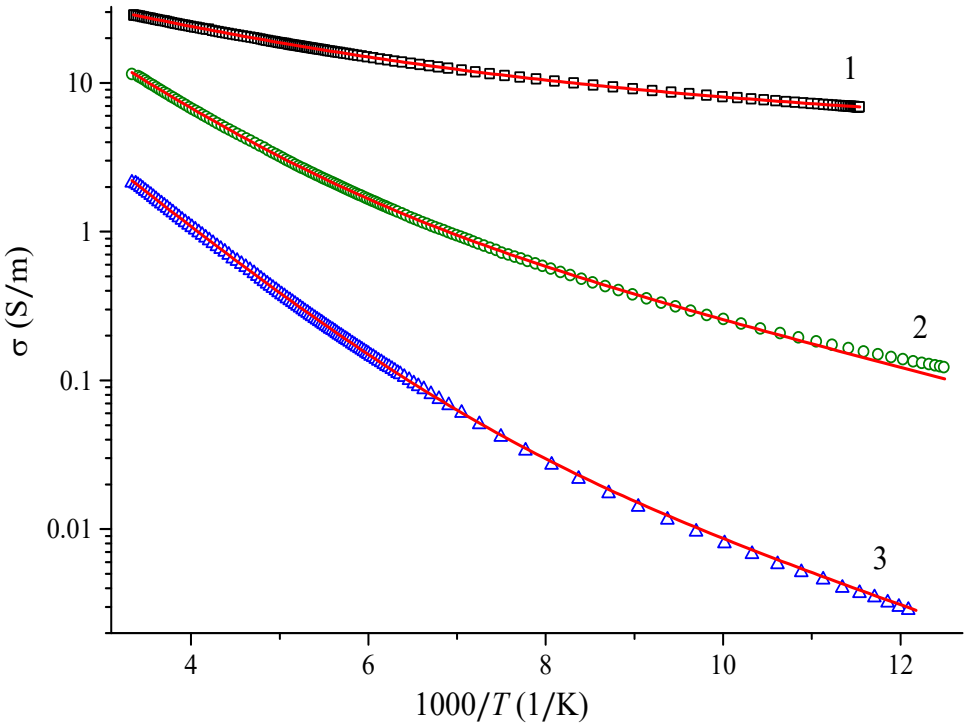

Figure 3 – Temperature dependences of the electrical conductivity in the scale σ(1/*T*) of the tin oxide films deposited by magnetron sputtering of tin onto glass substrates in an argon atmosphere, followed by two-stage annealing in air: at 200 °C for 2 hours at the 1st stage and at 350 (1), 400 (2) or 450 °C (3) for 1 hour at the 2nd stage. Solid lines are the results of the approximation of the experimental data by Eq. (4)

It is known that for crystalline semiconductors with activation type of σ(*T*) dependence the relationship between the Seebeck coefficient *S* and the position of the Fermi level E_F in the forbidden band is described by the Pisarenko's formula [28, 41, 42]:

$$S = -\frac{k_B}{e}(r + 5/2 - \eta), \quad (5)$$

where k_B is the Boltzmann constant; *e* is the elementary charge; $\eta = E_F/k_BT$ is the reduced Fermi energy. For crystalline semiconductors with a dominant mechanism of electron scattering on acoustic phonons, the parameter $r = -1/2$.

The Fermi level position calculated using Eq. (5) with $r = -1/2$ was found to be inconsistent with the measured temperature dependence of electrical conductivity σ(*T*) for our multiphase films. For example, for a film annealed at 350 °C, the Fermi level should be located above the bottom of the conduction band according to Eq. (5). The best correlation between the results of measurements of the σ(*T*)

dependences and the Seebeck coefficient was achieved with parameter values $r < -2$.

The calculated values of the Fermi level position in the band gap of our samples were found to be equal to −13.6, −32.7 and −34.8 meV in the case of parameter $r = -2$ and Seebeck coefficient S (measured at temperature $T \approx 300$ K) equal to −90, −156 and −163 μV/K for the tin oxides films annealed at 350, 400 and 450 °C, respectively. These Fermi level positions determined within the band gap of our samples show good agreement with the results obtained from electrical conductivity measurements. We assume that parameter r in Eq. (5), for amorphous and polycrystalline tin oxide multiphase samples with prevailing of SnO_2 phase, may differ from that of crystalline tin dioxide films due to additional charge and heat scattering mechanisms beyond acoustic phonons scattering.

Conclusion

The possibility of synthesis of disordered tin oxide films with amorphous and polycrystalline structure characterized by various values of electrical conductivity σ and Seebeck coefficient S by changing the annealing temperature during fabrication procedure was demonstrated.

Activation of electrons from impurity levels associated to the oxygen vacancies in different charge states in the band gap of tin oxide films was proposed as main charge transport mechanism both in amorphous and in polycrystalline samples. The activation energy of electrons from these impurity levels was estimated. It was demonstrated that for all types of the samples, the Pisarenko's formula can be applied to evaluate the relationship between the Seebeck coefficient S and the position of the Fermi level E_F if the parameter $r < -2$.

These results can contribute to the development of thermoelectricity theory in disordered and heterogeneous materials, as well as to the design of thermoelectric energy converters utilizing disordered semiconductors.

Acknowledgments

This work was supported by the Belarusian Republican Foundation for Fundamental Research (grant No. F22-UZB-056), Belarusian National Research Program "Material science, new materials and technologies" (subprogram "Nanomaterials and nanotechnologies", task No. 2.14.3), Belarusian National Research Program "Convergence-2025" (subprogram "Interdisciplinary research and new emerging technologies", task No. 3.02.1.4). The authors are grateful to Dr. S.V. Zlotski and Dr. V.I. Shimanskij for implementation of X-ray diffraction measurements as well as to Dr. O.V. Korolik for implementation of Raman spectra measurements.

References

1. Bell LE. Cooling, heating, generating power, and recovering waste heat with thermoelectric systems. Science. 2008;321:1457-1461.
DOI: 10.1126/science.1158899

2. Di Salvo FJ. Thermoelectric cooling and power generation. Science. 1999;285:703-706.
DOI: 10.1126/science.285.5428.703

3. Dmitriev AV, Zvyagin IP. Current trends in the physics of thermoelectric materials. Phys. Usp. 2010;53(8):789-803. **DOI:** 10.3367/UFNe.0180.201008b.0821

4. Zevalkink A. [et al.]. A practical field guide to thermoelectrics: Fundamentals, synthesis, and characterization. Applied Physics Reviews. 2018;5(2):021303. **DOI:** 10.1063/1.5021094

5. Yamamoto K. [et al.]. Thermoelectricity near Anderson localization transitions. Physical Review B. 2017;96(15):155201.
DOI: 10.1103/PHYSREVB.96.155201

6. Dresselhaus MS. [et al.]. New Directions for Low-Dimensional Thermoelectric Materials. Advanced Materials. 2007;19(8):1043-1053.
DOI: 10.1002/adma.200600527

7. Wang J. [et al.]. Low-Dimensional Nanomaterials for Thermoelectric Detection of Infrared and Terahertz Photons. In: Park CR (ed.) Advanced Thermoelectric Materials. Scrivener Publishing LLC; 2019:267-316.

8. Pennelli G, Dimaggio E, Masci A. Silicon Nanowires: A Breakthrough for Thermoelectric Applications. Materials. 2021;14(18):5305. **DOI:** 10.3390/ma14185305

9. Zheng Y. [et al.]. Defect engineering in thermoelectric materials: what have we learned? Chemical Society Reviews. 2021;50(16):9022-9054.
DOI: 10.1039/D1CS00347J

10. Bux SK. [et al.]. Nanostructured Bulk Silicon as an Effective Thermoelectric Material. Adv. Funct. Mater. 2009;19(15):2445-2452. **DOI:** 10.1002/adfm.200900250

11. Ohita H. Thermoelectrics based on strontium titanate. Mater. Today 2007;10:44-49.
DOI: 10.1016/S1369-7021(07)70244-4

12. Tritt TM, Subramanian MA. Thermoelectric Materials, Phenomena, and Applications: A Bird's Eye View. MRS Bull. 2006;31:188-198. **DOI:** 10.1557/mrs2006.44

13. Dmitriev AV. High doping effect on the thermoelectric properties of p-type lead telluride. Journal of Applied Physics. 2018;123:165707. **DOI:** 10.1063/1.5025766

14. Feng Y. [et al.]. Metal oxides for thermoelectric power generation and beyond. Adv. Compos. Hybrid Mater. 2018;1(1):114-126.
DOI: 10.1007/s42114-017-0011-4

15. Kim S. [et al.]. Transparent Amorphous Oxide Semiconductor as Excellent Thermoelectric Materials. Coatings. 2018;8(12):462.
DOI: 10.3390/coatings8120462

16. Batzill M, Diebold U. The surface and materials science of tin oxide. Progress in Surface Science. 2005;79(2-4):47-154.
DOI: 10.1016/j.progsurf.2005.09.002

17. Kíliç C, Zunger A. Origins of coexistence of conductivity and transparency in SnO_2. Phys. Rev. Lett. 2002;88(9):095501.
DOI: 10.1103/PhysRevLett.88.095501

18. Ksenevich V. [et al.]. Weak Localization in Polycrystalline Tin Dioxide Films. Materials. 2020;13(23):5415. **DOI:** 10.3390/ma13235415

19. Miller S. [et al.]. SnO as a Potential Oxide Thermoelectric Candidate. J. Mater. Chem. C. 2017;5(34): 8854-8861. **DOI:** 10.1039/C7TC01623A

20. Vieira EMF. [et al.]. Highly sensitive thermoelectric touch sensor based on p-type SnO_x thin film. Nanotechnology. 2019;30(43):5502.
DOI: 10.1088/1361-6528/ab33dd

21. Kuwahara S. Synthesis of High-Density Bulk Tin Monoxide and Its Thermoelectric Properties. Materials Transactions. 2018;59(7):1022-1029.
DOI: 10.2320/matertrans.E-M2018804

22. Kumar DA. [et al.]. Nanostructured Oxide (SnO_2, FTO) Thin Films for Energy Harvesting: A Significant Increase in Thermoelectric Power at Low Temperature. Micromachines. 2024;15(2):188. **DOI:** 10.3390/mi15020188

23. Bagheri-Mohagheghi M-M, Shokooh-Saremi M. The electrical, optical, structural and thermoelectrical characterization of n- and p-type cobalt-doped SnO_2 transparent semiconducting films prepared by spray pyrolysis technique. Phys. B Condens. Matter. 2010;405(19):4205-4210. **DOI:** 10.1016/j.physb.2010.06.067

24. Moharrami F, Bagheri-Mohagheghi M-M, Azimi-Juybari H. Study of structural, electrical, optical, thermoelectric and photoconductive properties of S and Al co-doped SnO_2 semiconductor thin films prepared by spray pyrolysis. Thin Solid Film. 2012;520(21):6503-6509. **DOI:** 10.1016/j.tsf.2012.06.075

25. Ferreira M. [et al.]. SnO_2 thin film oxides produced by rf sputtering for transparent thermoelectric devices. Mater. Today Proc. 2015;2(2):647-653.
DOI: 10.1016/j.matpr.2015.05.090

26. Macario LR, Golabek A, Kleinke H, Leite ER. Thermoelectric properties of Sb-doped tin oxide by a one-step solid-state reaction. Ceramics International. 2022;48(3): 3585-3591.
DOI: 10.1016/j.ceramint.2021.10.137

27. Walsh A, Watson GW. Influence of the anion on lone pair formation in Sn(II) monochalcogenides: A DFT study. Journal of Physical Chemistry B. 2005;109(40):18868-18875. **DOI:** 10.1021/jp051822r

28. Seeger K. Physics of Semiconductors M., Mir. 1977;615 p.

29. Adamchuck DV, Ksenevich VK, Gorbachuk NI, Shimanskij VI. Impedance spectroscopy of polycrystalline tin dioxide films. Devices and Methods of Measurements. 2016;7(3):312-321. (In Russ.)
DOI: 10.21122/2220-9506-2016-7-3-84-89

30. Adamchuck DV, Ksenevich VK. Control of Electrical and Optical Parameters of Humidity Sensors Active Elements Based on Tin Oxides Films with Variable Composition. Devices and Methods of Measurements. 2019;10(2):138-150. (In Russ.)
DOI: 10.21122/2220-9506-2019-10-2-138-150

31. Adamchuk DV. [et al.]. Nonstoichiometric tin oxide films: study by X-ray diffraction, Raman scattering and electron paramagnetic resonance. Lithuanian Journal of Physics. 2019;59(4):179-187.
DOI: 10.3952/physics.v59i4.4138

32. Adamchuck DV, Ksenevich VK, Poklonski NA, Kavaleu AI. Features of water vapor adsorption and desorption on the surface of non-stoichiometric tin dioxide films. Vestsi Natsyianal'nai akademii navuk Belarusi. Seryia fizika-matematychnykh navuk = Proceedings of the National Academy of Sciences of Belarus. Physics and Mathematics series. 2020;56(1):102-113. (in Russ.)
DOI: 10.29235/1561-2430-2020-56-1-102-113

33. Ksenevich VK. [et al.]. Effect of the oxidative annealing temperature on the structural and optical characteristics of tin oxide films. Journal of Applied Spectroscopy. 2025;91(6):1233-1239.
DOI: 10.1007/s10812-025-01842-z

34. Ksenevich V. [et al.]. Synthesis of amorphous and polycrystalline tin oxide films for applications as thermoelectric materials. Interaction of Radiation with Solids : Proceedings of the 15th International Conference, Minsk, Belarus, September 26-29, 2023 / Belarusian State Univ.; ed.: V.V. Uglov (ed.-in-chief) [et al.]. Minsk, BSU. 2023;521-523 (In Russ.). https://elib.bsu.by/handle/123456789/304265

35. Boroojerdian P. Structural and Optical Study of SnO Nanoparticles Synthesized Using Microwave–Assisted Hydrothermal Route // International Journal of Nanoscience and Nanotechnology. 2013;9(2):95-100. https://www.ijnnonline.net/article_3824.html

36. Sangaletti L. [et al.] Oxidation of Sn thin films to SnO_2. Micro-raman mapping and X-ray diffraction studies // Journal of Materials Research. 1998;13(9):2457-2460. **DOI:** 10.1557/JMR.1998.0343.

37. Eifert B. [et al.]. Raman studies of the intermediate tin-oxide phase. Physical Review Materials 2017;1:014602.
DOI: 10.1103/PhysRevMaterials.1.014602

38. Jiang J. [et al.]. Transport mechanisms in SnO_2: N, H thin film grown by chemical vapor deposition. Phys. Status Solidi B: Basic Research. 2017;254(7):1700003. **DOI:** 10.1002/pssb.201700003

39. Ji YC, Zhang HX, Zhang XH, Li ZQ. Structures, optical properties, and electrical transport processes of SnO_2 films with oxygen deficiencies. Phys. Stat. Sol. (B). 2013;250(10):2145-2152.
DOI: 10.1002/pssb.201349086

40. Samson S, Fonstad CG. Defect structure and electronic donor levels in stannic oxide crystals. J. Appl. Phys. 1973;44(10):4618-4621.
DOI: 10.1063/1.1662011

41. Serhiienko I. [et al.]. Record-High Thermoelectric Performance in Al-Doped ZnO via Anderson Localization of Band Edge States. Adv. Sci. 2024;11:2309291. DOI: 10.1002/advs.202309291

42. Novitskii A. [et al.]. Defect Engineering of Bi_2SeO_2 Thermoelectrics. Adv. Funct. Mater. 2025;35:2416509. **DOI:** 10.1002/adfm.202416509